

4

DTIC FILE COPY

AFGL-TR-88-0033  
ENVIRONMENTAL RESEARCH PAPERS, NO. 995

AD-A196 324

Long-Range Seismic Recording of the MISTY PICTURE High  
Explosive Test, White Sands Missile Range, New Mexico

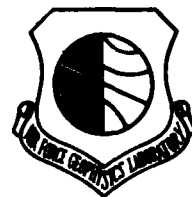
JOHN CIPAR



4 February 1988



Approved for public release; distribution unlimited.



EARTH SCIENCES DIVISION

PROJECT 2309


**AIR FORCE GEOPHYSICS LABORATORY**

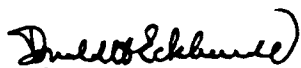
HANSCOM AFB, MA 01731

DTIC  
ELECTE  
JUL 27 1988  
S H D

This technical report has been reviewed and is approved for publication.

FOR THE COMMANDER

  
HENRY A. OSSING, Chief  
Solid Earth Geophysics Branch

  
DONALD H. ECKHARDT  
Director  
Earth Sciences Division

This document has been reviewed by the ESD Public Affairs Office (PA) and is releasable to the National Technical Information Service (NTIS).

Qualified requestors may obtain additional copies from the Defense Technical Information Center. All others should apply to the National Technical Information Service.

If your address has changed, or if you wish to be removed from the mailing list, or if the addressee is no longer employed by your organization, please notify AFGL/DAA, Hanscom AFB, MA 01731. This will assist us in maintaining a current mailing list.

REPORT DOCUMENTATION PAGE				
1a. REPORT SECURITY CLASSIFICATION Unclassified		1b. RESTRICTIVE MARKINGS		
2a. SECURITY CLASSIFICATION AUTHORITY		3. DISTRIBUTION / AVAILABILITY OF REPORT Approved for public release; distribution unlimited.		
2b. DECLASSIFICATION / DOWNGRADING SCHEDULE				
4. PERFORMING ORGANIZATION REPORT NUMBER(S) AFGL-TR-88-0033 ERP, No. 995		5. MONITORING ORGANIZATION REPORT NUMBER(S)		
6a. NAME OF PERFORMING ORGANIZATION Air Force Geophysics Laboratory	6b. OFFICE SYMBOL (if applicable) LWH	7a. NAME OF MONITORING ORGANIZATION		
6c. ADDRESS (City, State, and ZIP Code) Hanscom AFB Massachusetts 01731-5000		7b. ADDRESS (City, State, and ZIP Code)		
8a. NAME OF FUNDING / SPONSORING ORGANIZATION AF Office of Scientific Res.	8b. OFFICE SYMBOL (if applicable) AFOSR/NP	9. PROCUREMENT INSTRUMENT IDENTIFICATION NUMBER		
8c. ADDRESS (City, State, and ZIP Code) Bolling AFB Washington, DC 20332		10. SOURCE OF FUNDING NUMBERS		
		PROGRAM ELEMENT NO. 61102F	PROJECT NO. 2309	TASK NO. G2
				WORK UNIT ACCESSION NO. 04
11. TITLE (Include Security Classification) Long-Range Seismic Recording of the MISTY PICTURE High Explosive Test, White Sands Missile Range, New Mexico				
12. PERSONAL AUTHOR(S) Cipar, John				
13a. TYPE OF REPORT Scientific Interim	13b. TIME COVERED FROM Feb 87 to Feb 88	14. DATE OF REPORT (Year, Month, Day) 1988 February 4	15. PAGE COUNT 32	
16. SUPPLEMENTARY NOTATION Also published in DNA "MISTY PICTURE" Symposium volume				
17. COSATI CODES		18. SUBJECT TERMS (Continue on reverse if necessary and identify by block number)		
FIELD	GROUP	SUB-GROUP		
		→ high explosive tests; chemical explosions, seismology; seismic waves; crustal structure. (Add) ←		
19. ABSTRACT (Continue on reverse if necessary and identify by block number) The Solid Earth Geophysics Branch of the Air Force Geophysics Laboratory recorded the MISTY PICTURE high explosive test at nine sites in the Tularosa Basin of southern New Mexico. Each site consisted of a three component seismometer set and a digital event recorder. The stations were due south of the explosion between 95 and 127 km. Analysis of P-wave travel times indicates that the crust is 30-32 km thick beneath the Tularosa Basin, a side graben of the Rio Grande Rift. S-wave travel times are consistent with earlier surface wave results. Polarization analysis indicates complex scattered and converted energy between the P- and S-wave groups.				
20. DISTRIBUTION / AVAILABILITY OF ABSTRACT <input checked="" type="checkbox"/> UNCLASSIFIED/UNLIMITED <input checked="" type="checkbox"/> SAME AS RPT <input type="checkbox"/> DTIC USERS		21. ABSTRACT SECURITY CLASSIFICATION Unclassified		
22a. NAME OF RESPONSIBLE INDIVIDUAL John J. Cipar		22b. TELEPHONE (Include Area Code) (617) 377-3746	22c. OFFICE SYMBOL AFGL/LWH	

## Contents

1. MISTY PICTURE SEISMIC EXPERIMENT	1
2. TULAROSA BASIN SEISMIC ARRAY	2
3. SEISMIC RECORD SECTIONS	5
4. POLARIZATION ANALYSIS	6
5. CONCLUSION	6
REFERENCES	7
APPENDIX	9

## Illustrations

1. Map of the Rio Grande Rift	11
2. Map of the Tularosa Valley	12
3-11. MISTY PICTURE Seismograms	13-21
12. Vertical record section	22
13. Radial record section	23
14. Transverse record section	24
15. Vertical times radial product record section	25



Accession For	
NTIS GRA&I	<input checked="" type="checkbox"/>
DTIC TAB	<input type="checkbox"/>
Unannounced	<input type="checkbox"/>
Justification	
By _____	
Distribution/	
Availability Codes	
Dist	Avail and/or Special
A-1	

## Tables

1. MISTY PICTURE Seismic Stations	2
2. Seismometer Constants	3
3. DCS-302 Recorder Constants	4
4. MISTY PICTURE Station Clock Corrections	5

## **Long-Range Seismic Recording of the MISTY PICTURE High Explosive Test, White Sands Missile Range, New Mexico**

### **1. MISTY PICTURE SEISMIC EXPERIMENT**

The Defense Nuclear Agency (DNA) has a long standing program of high explosive experiments to test the design of systems in a simulated nuclear overpressure environment. The MISTY PICTURE high explosive experiment, the most recent of these tests, involved detonating a 4880-ton charge of ammonium nitrate mixed with fuel oil (ANFO), contained in a 27-meter diameter hemispherical container at ground level. This provided an airblast approximately equivalent to an 8-kiloton (kt) nuclear device. The experiment was conducted at the Defense Nuclear Agency Permanent High Explosive Test Station located in the Jornada del Muerto portion of White Sands Missile Range, New Mexico (WSMR). Relevant seismological parameters for the MISTY PICTURE test are given in Table 1.

The large size of the shot, as well as its location in the southern section of the Rio Grande Rift made it an ideal source for seismic crustal structure studies. Recordings of previous DNA shots such as MINOR SCALE<sup>1</sup> indicated that excellent seismic measurements could be obtained. The Rio Grande Rift is an active continental rift zone stretching from the United States-Mexican border to central Colorado (Figure 1). The rift is characterized by recent geodetic deformation, high heat flow, moderate

---

(Received for Publication 20 January 1988)

1. Kirchoff, S. (1986) Crustal structure beneath the Tularosa Basin in the White Sands Missile Range, New Mexico, MS Thesis, Boston University.

seismicity, and crustal thinning.<sup>2</sup> Sinno et al<sup>3</sup> infer that the crust in the southern rift is approximately 30 kilometers (km) thick. This report will describe seismic data recorded east of the Sinno et al<sup>3</sup> profile, in the Tularosa Valley, west of Alamogordo, New Mexico (Figure 2).

Table 1. MISTY PICTURE Seismic Stations

Date	Origin	Time	Latitude	Longitude	Depth	Elevation	
May 14, 1987	134D 16H OM	0.031S	33.620N	106.474W	0.0	1504.0	
Location: MISTY PICTURE, White Sands Missile Range, New Mexico							
Station	Latitude (Deg)	Longitude (Deg)	Elevation (Meters)	Delta (Deg)	Distance (Km)	Azimuth (Deg)	Back Azimuth (Deg)
MPO1 250 AFGL	33.155N	106.488W	1225.00	0.464	51.59	181.45	1.44
MPO2 117 AFGL	33.125N	106.506W	1220.00	0.494	54.98	183.11	3.10
MPO3 248 AFGL	33.079N	106.531W	1215.00	0.542	60.24	185.07	5.04
MPO4 122 AFGL	33.016N	106.519W	1200.00	0.604	67.12	183.59	3.57
MPO5 274 AFGL	32.956N	106.516W	1200.00	0.663	73.75	183.05	3.03
MPO6 0 AFGL	32.911N	106.514W	1200.00	0.708	78.72	182.72	2.70
MPO7 0 AFGL	32.871N	106.489W	1225.00	0.747	83.08	180.97	0.96
MPO8 0 AFGL	32.822N	106.488W	1225.00	0.796	88.51	180.85	0.84
MPO9 0 AFGL	32.780N	106.482W	1235.00	0.838	93.17	180.46	0.46
MP10 311 AFGL	32.746N	106.467W	1235.00	0.872	96.93	179.61	359.62
MP11 332 AFGL	32.717N	106.467W	1220.00	0.901	100.15	179.62	359.63
MP12 333 AFGL	32.689N	106.467W	1220.00	0.928	103.26	179.64	359.64
MP13 302 AFGL	32.663N	106.460W	1245.00	0.954	106.14	179.29	359.30
MP14 301 AFGL	32.636N	106.445W	1265.00	0.982	109.16	178.57	358.59
MP15 309 AFGL	32.609N	106.424W	1240.00	1.009	112.22	177.60	357.63
MP16 284 AFGL	32.583N	106.430W	1250.00	1.035	115.08	177.94	357.97
MP17 300 AFGL	32.555N	106.425W	1220.00	1.063	118.20	177.77	357.80
MP18 279 AFGL	32.531N	106.424W	1255.00	1.087	120.87	177.77	357.80
MP19 299 AFGL	32.507N	106.425W	1245.00	1.111	123.52	177.86	357.89
MP20 334 AFGL	32.482N	106.425W	1220.00	1.136	126.29	177.91	357.94

## 2. TULAROSA BASIN SEISMIC ARRAY

Portable digital seismographs were installed along WSMR Route 7 from Rhodes Canyon Range Center south to the junction of Route 7 and U. S. Highway 70 (Figure 2). The array was aligned nearly due south of the test site, at roughly 50 to 125 km distance.

Four organizations participated in this portion of the experiment: Air Force Geophysics Laboratory (AFGL), Air Force Weapons Laboratory (AFWL), SUNY at Binghamton, and the University of North Carolina (UNC) (see the Appendix for list of participants). The SUNY group attempted to record with accelerometers, but accelerations were too low at 50 km to trigger the recorders. None of the instruments at stations 1 through 10 recorded the shot. Recorders at stations 15 and 16 failed to

2. Cordell, L. (1978) Regional geophysical setting of the Rio Grande Rift, *Bull. Geol. Soc. Am.* **89**:7:1073-1090.
3. Sinno, Y.A., Daggett, P.H., Keller, G.R., Morgan, P., and Harder, S.H. (1986) Crustal structure of the Southern Rio Grande Rift determined from seismic refraction profiling, *J. Geophys. Res.* **91**:B6:6143-6156.

trigger and thus missed the shot. However, excellent seismograms were obtained from stations 10 through 14 and 17 through 20 (Figures 3 through 11).

Each working station consisted of a Terra Technology DCS-302 digital seismic recorder and a Sprengnether Instruments S-6000 triaxial seismometer. Data was recorded on cassette tapes at 100 samples/second. The recorder response is flat from DC to the anti-aliasing filter cutoff frequency. Above the cutoff frequency the response rolls off at 6 dB/octave using a 6-pole Butterworth filter. The DCS-302 recorders have automatic gain ranging over four gain settings. At a given gain, recorder sensitivity is given by:  $[(5.0 \text{ volts})/(2048 \text{ counts})]/(\text{gain})$ . This data is given in Table 3. The recorder-seismometer installations could not be calibrated in the field; however, calibrations performed for a subsequent experiment were used in decoding the data.<sup>4</sup> Seismometer data is given in Table 2. The

Table 2. Seismometer Constants

Seismogram	Time Correction (Seconds)	Seismometer Orientation (Degrees)	Seismometer Sensitivity (Volts/M/Sec)	Pendulum Period (Seconds)	Damping Ratio	Serial Number
MP10 MSTY SPZ	-0.0039	-	238.9405	0.178	0.442	6842
MP10 MSTY SPN	-0.0039	12.30	264.7592	0.481	0.475	6842
MP10 MSTY SPE	-0.0039	102.30	240.8680	0.481	0.426	6842
MP11 MSTY SPZ	0.0043	-	238.9405	0.478	0.442	6842
MP11 MSTY SPN	0.0043	12.30	264.7592	0.481	0.475	6842
MP11 MSTY SPE	0.0043	102.30	240.8680	0.481	0.426	6842
MP12 MSTY SPZ	0.0020	-	175.8188	0.437	0.366	8294
MP12 MSTY SPN	0.0020	12.30	147.3650	0.517	0.386	8294
MP12 MSTY SPE	0.0020	102.30	157.9338	0.544	0.451	8294
MP13 MSTY SPZ	2.0079	-	147.7618	0.430	0.317	7493
MP13 MSTY SPN	2.0079	12.30	171.2903	0.498	0.413	7493
MP13 MSTY SPE	2.0079	102.30	152.6692	0.497	0.426	7493
MP14 MSTY SPZ	0.0078	-	163.1083	0.453	0.438	6844
MP14 MSTY SPN	0.0078	12.30	164.7215	0.503	0.514	6844
MP14 MSTY SPE	0.0078	102.30	171.8547	0.494	0.491	6844
MP17 MSTY SPZ	0.0038	-	170.1989	0.375	0.323	8295
MP17 MSTY SPN	0.0038	12.30	169.0932	0.491	0.403	8295
MP17 MSTY SPE	0.0038	102.30	177.2410	0.479	0.379	8295
MP18 MSTY SPZ	0.0039	-	163.3998	0.400	0.330	7679
MP18 MSTY SPN	0.0039	12.30	159.7791	0.481	0.386	7679
MP18 MSTY SPE	0.0039	102.30	157.3085	0.496	0.413	7679
MP19 MSTY SPZ	0.0135	-	177.3931	0.452	0.458	6843
MP19 MSTY SPN	0.0135	12.30	175.5116	0.494	0.502	6843
MP19 MSTY SPE	0.0135	102.30	177.5222	0.501	0.510	6843
MP20 MSTY SPZ	0.0542	-	151.3522	0.442	0.357	7680
MP20 MSTY SPN	0.0542	12.30	145.8752	0.498	0.389	7680
MP20 MSTY SPE	0.0542	102.30	155.7216	0.459	0.370	7680

triaxial seismometers were aligned with the longitudinal axis pointed to magnetic north. Declination in this area is 12.3 east of geographic north. Since MISTY PICTURE is almost due north of the station array, the north-south component recorded nearly pure radial motion. Stations were located as far as

4. Hussey, V., private communication.

practical at known landmarks such as road junctions. Latitude, longitude, and elevations were read from U.S. Geological Survey 1:100,000 metric topographic maps (Table 1).

Each recorder has an internal clock that can be set prior to the experiment to Universal Time (UTC) provided by an external time reference, a Kinematics 468-DC GEOS satellite clock. As soon as possible after the experiment, the clocks were checked for drift relative to the satellite clock. The drift is measured as "slew", the number of digital sample intervals between the external time reference and the recorder internal second pulse. The time corrections given in Tables 2 and 4 are the corrections to be added to the recorder time to correct to UTC. Starting times given in Figures 3 through 11 have been corrected to UTC.

Table 3. DCS-302 Recorder Constants

Seismogram	Cut-Off Frequency (Hertz)	Recorder Gains (Millivolts/Count)				Serial Number
		Gain 1	Gain 2	Gain 3	Gain 4	
MP10 MSTY SPZ	30.00	2.44141	0.48828	0.09766	0.02441	311
MP10 MSTY SPN	30.00	2.44141	0.48828	0.09766	0.02551	311
MP10 MSTY SPE	30.00	2.44141	0.48828	0.09766	0.02441	311
MP11 MSTY SPZ	30.00	2.44141	0.48828	0.09766	0.02441	332
MP11 MSTY SPN	30.00	2.44141	0.48828	0.09766	0.02441	332
MP11 MSTY SPE	30.00	2.44141	0.48828	0.09666	0.02441	332
MP12 MSTY SPZ	30.00	2.44141	0.48828	0.09666	0.02441	333
MP12 MSTY SPN	30.00	2.44141	0.48828	0.09766	0.02441	333
MP12 MSTY SPE	30.00	2.44141	0.48828	0.09766	0.02441	333
MP13 MSTY SPZ	30.00	2.44141	0.48828	0.09766	0.02441	302
MP13 MSTY SPN	30.00	2.44141	0.48828	0.09766	0.02441	302
MP13 MSTY SPE	30.00	2.44141	0.48828	0.09766	0.02441	302
MP14 MSTY SPZ	30.00	2.44141	0.48828	0.09766	0.02441	301
MP14 MSTY SPN	30.00	2.44141	0.48828	0.09766	0.02441	301
MP14 MSTY SPE	30.00	2.44141	0.48828	0.09766	0.02441	301
MP17 MSTY SPZ	30.00	2.44141	0.48828	0.09766	0.02441	300
MP17 MSTY SPN	30.00	2.44141	0.48828	0.09766	0.02441	300
MP17 MSTY SPE	30.00	2.44141	0.48828	0.09766	0.02441	300
MP18 MSTY SPZ	30.00	0.24414	0.04883	0.00977	0.00244	279
MP18 MSTY SPN	30.00	0.24414	0.04883	0.00977	0.00244	279
MP18 MSTY SPE	30.00	0.24414	0.04883	0.00977	0.00244	279
MP19 MSTY SPZ	30.00	2.44141	0.48828	0.09766	0.02441	299
MP19 MSTY SPN	30.00	2.44141	0.48828	0.09766	0.02441	299
MP19 MSTY SPE	30.00	2.44141	0.48828	0.09766	0.02441	299
MP20 MSTY SPZ	30.00	0.25326	0.04907	0.00970	0.00245	334
MP20 MSTY SPN	30.00	0.25511	0.04952	0.00980	0.00246	334
MP20 MSTY SPE	30.00	0.25564	0.04973	0.00981	0.00242	334

Table 4. MISTY PICTURE Station Clock Corrections

Station	Recorder	Slew*	Time (UTC)	Clock Correction (sec)
MP01	250	048	19h 14m	
MP02	117	no slew, appears correct		
MP03	248	recorder stopped		
MP04	122	no display		
MP05	274	OC 2	19h 01m	
MP10	311	298	17h 40m	0.0039
MP11	332	003	19h 02m	
MP12	333	299	17h 38m	0.0020
MP13	302	004	17h 37m	2.0079
	(recorder 302 is 2 sec slow)			
MP14	301	004	17h 38m	0.0078
MP15	309	000/299	17h 36m	0.0000
MP16	284	286	17h 45m	0.0267
MP17	300	298	17h 45m	0.0038
MP18	279	298	17h 42m	0.0039
MP19	299	293	17h 42m	0.0135
	(recorder set to Mountain Daylight Time)			
MP20	334	028	17h 41m	0.0542

\*Records initially set at 13 h 00m

### 3. SEISMIC RECORD SECTIONS

Record sections for the vertical, radial, and transverse component seismograms are plotted in Figures 12, 13, and 14 at a reduction velocity of 5.0 km/sec. Travel time curves for an assumed crustal model are shown for reference. Model parameters are given in the upper left. The S-wave structure is adapted from a surface wave model of Sinno and Keller.<sup>5</sup> The P-wave model was derived by fitting travel times of the major arrivals and further constrained by using generalized ray synthetics to fit relative amplitudes.

The small first arrival at each station on the vertical section (Figure 12) is Pg, a P-wave refracted along the sediment-upper crust interface. This wave has an apparent velocity across the array of just under 6.0 km/sec. The most prominent arrival on the vertical seismogram is PmP, the P-wave reflection from the crust-mantle boundary (Moho). Because of its high phase velocity, PmP gradually moves to the front of the seismogram with increasing distance. The distance at which PmP becomes a critical reflection is approximately 85 km for this model. A small Pn wave refracted along the crust-mantle boundary leads PmP over the array aperture.

Between Pg and PmP is at least one, and possibly two, additional arrivals. These are probably refractions along boundaries in the middle and lower crust. The P(6.10) arrival has an apparent phase velocity of 6.10 km/sec. A weak arrival of phase velocity 6.5 km/sec is also indicated.

5. Sinno, Y.A. and Keller, G.R. (1986) A Rayleigh wave dispersion study between El Paso, Texas and Albuquerque, New Mexico, *J. Geophys. Res.* **91**:B6:6168-6174.

The S-wave travel time curves are shown at right. Clearly there are no coherent arrivals corresponding to the upper and middle crustal layers. The data indicate a highly variable arrival about the expected SmS time. The radial record section (Figure 13) shows a slightly more coherent SmS arrival, as expected, yet not nearly as well defined as the vertical PmP.

Note the high amplitude arrivals between the P- and S-wave groups on the radial component. There are no obvious phase velocity relationships across the array for any of these waves; this suggests they are signal-generated noise scattered from heterogeneities near the stations.

The long-period energy arriving after SmS appears to be Rayleigh surface waves. The lack of coherence is somewhat surprising, suggesting strong multipathing and scattering. The transverse record section (Figure 14) shows little or no coherence among arrivals.

#### 4. POLARIZATION ANALYSIS

The availability of three component seismograms allows examination of the polarization state of each arrival. A pure P-wave is polarized in the direction of propagation; that is, the vertical and radial components should be in phase. Alternatively, an S-wave is polarized orthogonal to the direction of propagation, and the vertical and radial are 180° out of phase. A Rayleigh wave has a 90° phase shift between radial and vertical components. Sutton and Pomeroy<sup>6</sup> suggest that a seismogram that is the product of the radial and vertical records would distinguish each arrival. On a product seismogram, the P-wave arrivals would be positive, SV negative, and Rayleigh waves oscillating. A product record section is shown in Figure 15. The PmP arrival stands out as clear positive motion. More interesting, the SmS is at best ambiguous suggesting that this arrival is an SmS-to-P conversion in the upper crust under the station. There is clearly an increase in signal at about the SmS time, but exactly what path this energy takes is unclear.

The large arrivals after PmP are also highly variable. For example, station MP11 shows prominent S energy arriving just after PmP (at about 1 sec reduced time); MP14 has a P followed by S; and MP18 shows a Rayleigh arrival.

#### 5. CONCLUSION

The three component seismic measurements of MISTY PICTURE indicate that the crust is approximately 30 to 32 km thick beneath the Tularosa Basin, in good agreement with Sinno et al<sup>3</sup>. Unlike the clear PmP arrival, SmS is poorly defined and may be a kind of converted phase. The complex structure beneath the stations leads to considerable incoherently scattered arrivals, including signal generated Rayleigh waves.

---

6. Sutton, G.H. and Pomeroy, P.W. (1963) Analog analyses of seismograms recorded on magnetic tape, *J. Geophys. Res.* **68**:9:2791-2815.

## References

1. Kirchoff, S. (1986) Crustal structure beneath the Tularosa Basin in the White Sands Missile Range, New Mexico, MS Thesis, Boston University.
2. Cordell, L. (1978) Regional geophysical setting of the Rio Grande Rift , *Bull. Geol. Soc. Am.* **89**:7:1073-1090.
3. Sinno, Y.A., Daggett, P.H., Keller, G.R., Morgan, P., and Harder, S.H. (1986) Crustal structure of the Southern Rio Grande Rift determined from seismic refraction profiling, *J. Geophys. Res.* **91**:B6:6143-6156.
4. Hussey, V., Private communication.
5. Sinno, Y.A. and Keller, G.R. (1986) A Rayleigh wave dispersion study between El Paso, Texas and Albuquerque, New Mexico, *J. Geophys. Res.* **91**:B6:6168-6174.
6. Sutton, G.H. and Pomeroy, P.W. (1963) Analog analyses of seismograms recorded on magnetic tape, *J. Geophys. Res.* **68**:9:2791-2815.

## **Appendix**

### **Participating Organizations and Personnel**

Solid Earth Geophysics Branch (AFGL/LWH)  
Earth Sciences Division  
Air Force Geophysics Laboratory  
Hanscom AFB, MA 01731  
John J. Cipar  
Joseph H. Craig, AIC  
Michael L. Hines, Capt.

Civil Engineering Research Division (AFWL/NTESG)  
Air Force Weapons Laboratory  
Kirtland AFB, NM 87117  
John Leverette  
David Fernald

Department of Geological and Environmental Sciences  
SUNY at Binghamton  
Binghamton, NY 13901  
Francis T. Wu  
Thomas Petruzzelli

Department of Geology  
University of North Carolina at Chapel Hill  
Chapel Hill, NC 27514  
Mark W. Martin



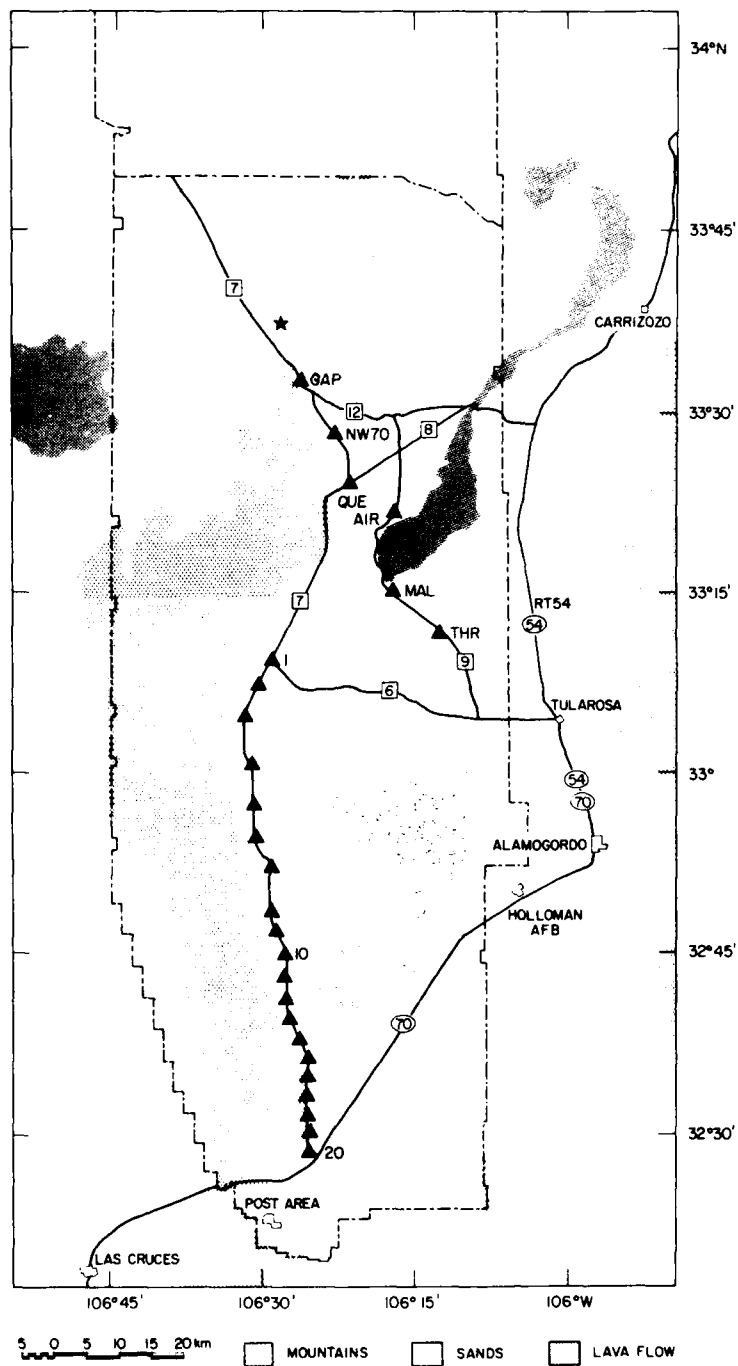
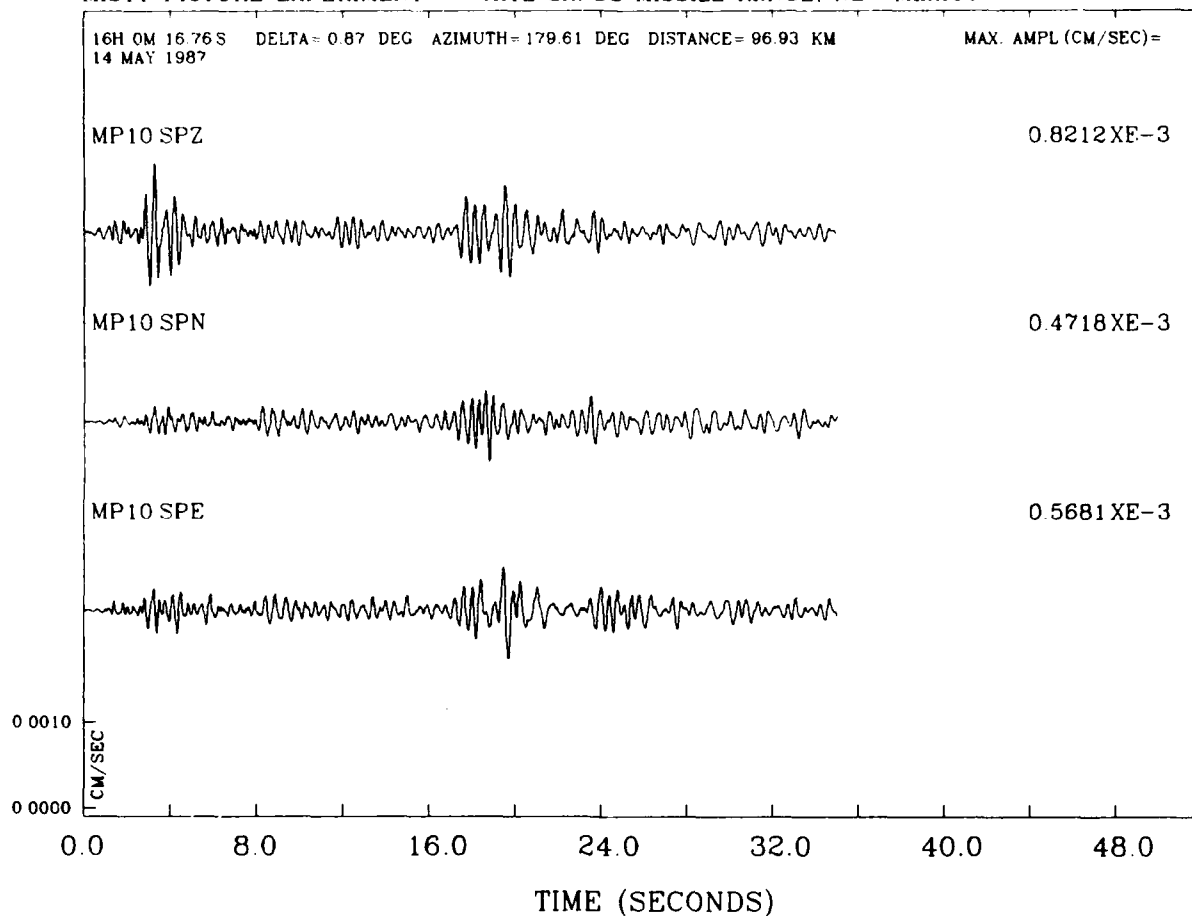


Figure 2. Map of the Tularosa Valley and adjacent mountain ranges showing the location of the MISTY PICTURE test (star) and seismic station array (triangles). Stations along WSMR Route 7 were occupied for MISTY PICTURE; others occupied during the June 1985 MINOR SCALE test.

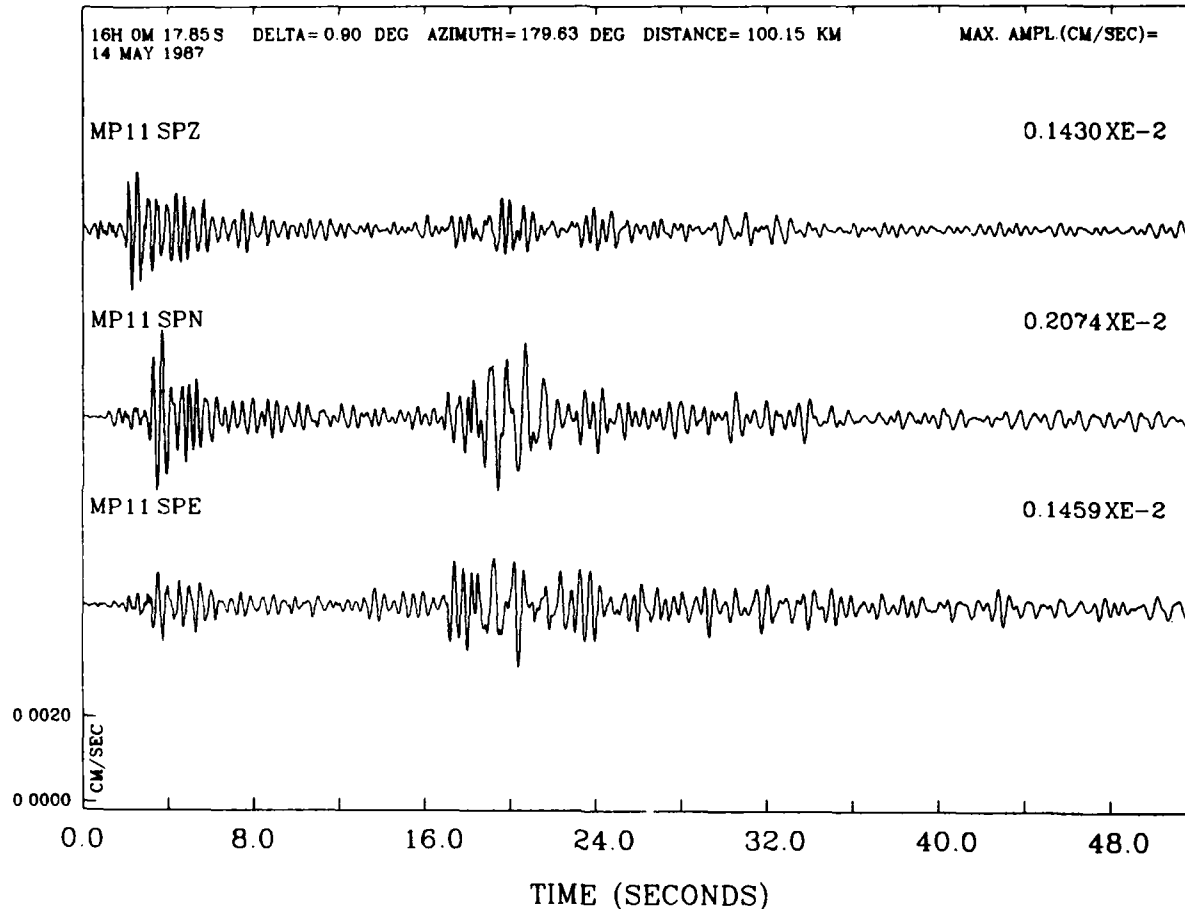
MISTY PICTURE EXPERIMENT - WHITE SANDS MISSILE RANGE, NEW MEXICO



4-NOV-87 10-41-31

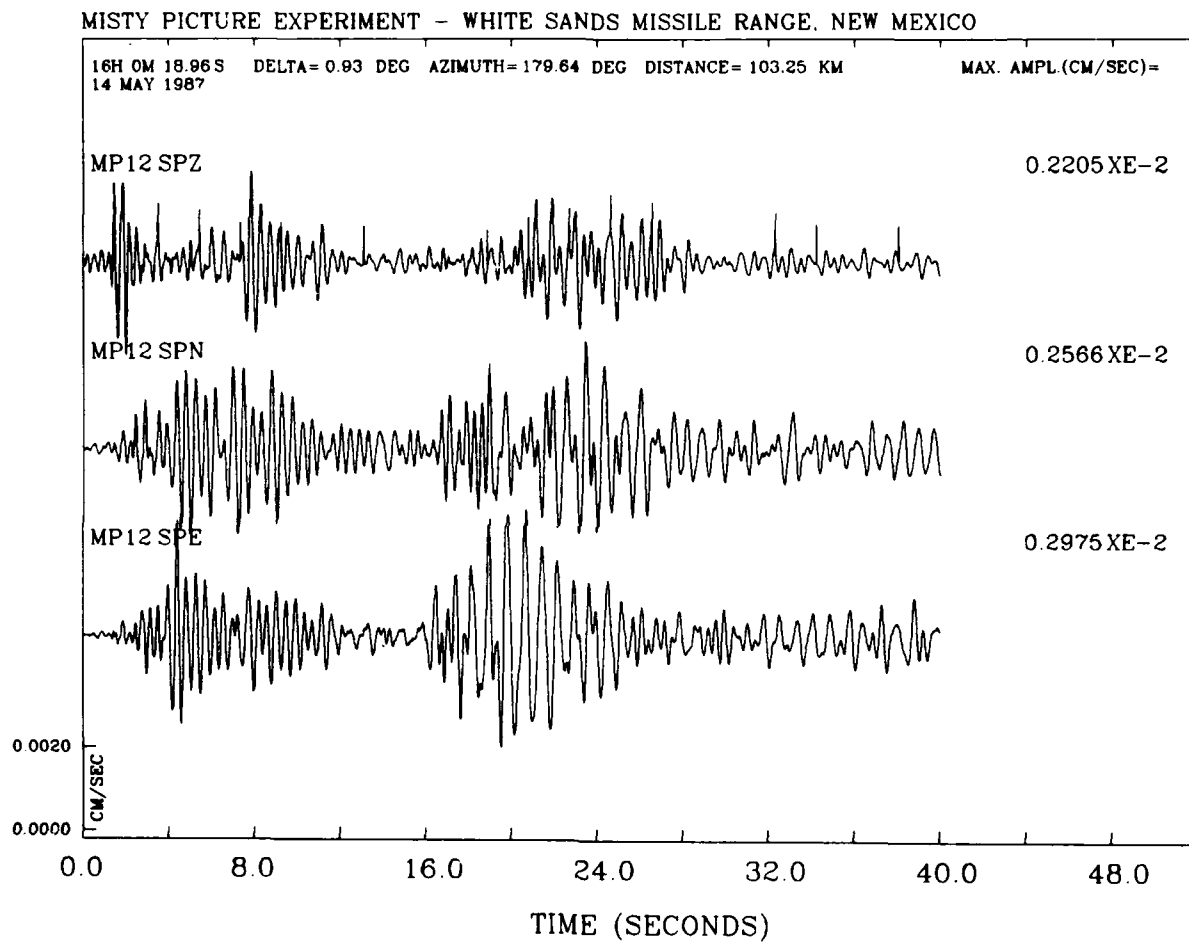
Figure 3. Seismograms recorded at station MP10 of the MISTY PICTURE array. Starting time (UTC) is given in the upper-left corner. Amplitude scale in cm/sec is shown at lower left with maximum amplitude displayed at the right of each trace.

# MISTY PICTURE EXPERIMENT - WHITE SANDS MISSILE RANGE, NEW MEXICO



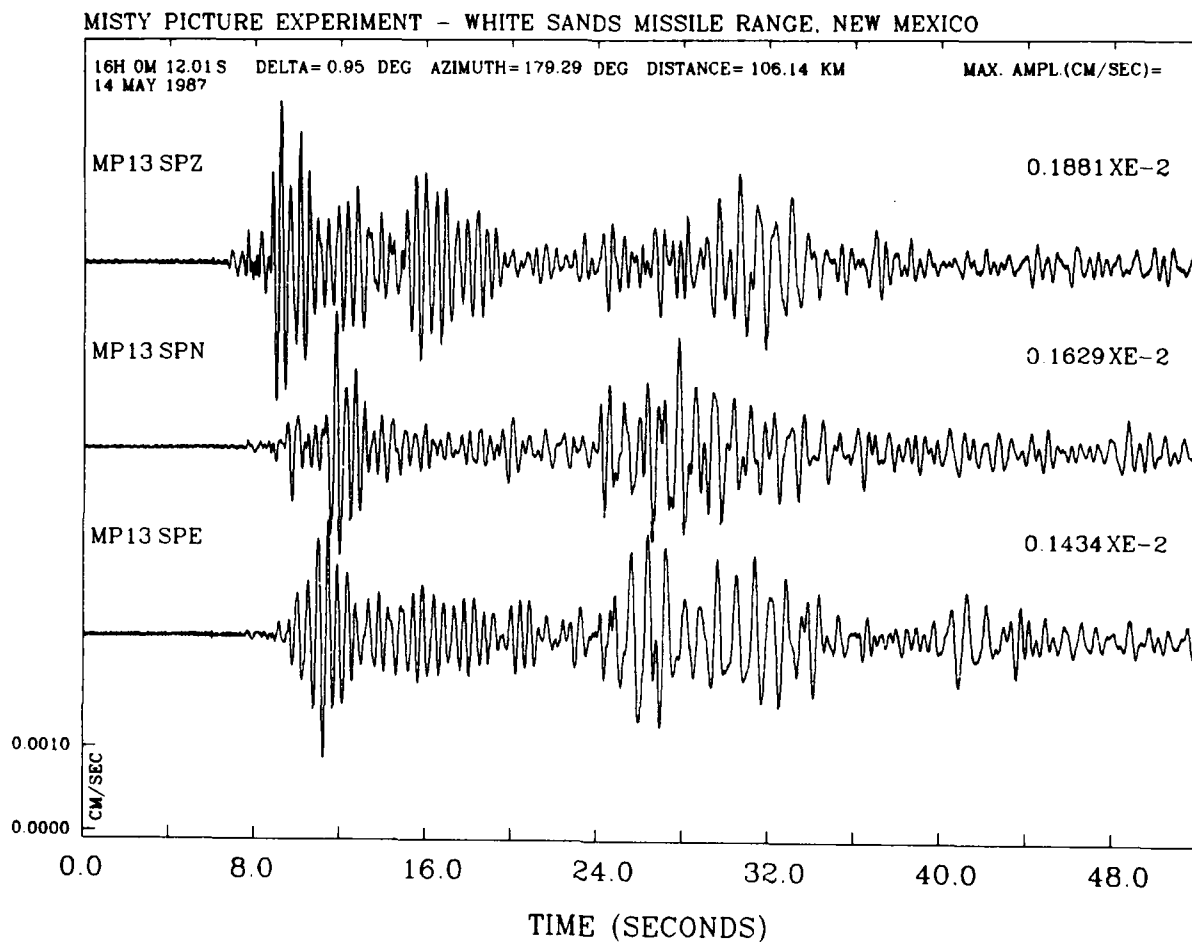
4-NOV-87 10-42-52

Figure 4. Seismograms recorded at station MP11 of the MISTY PICTURE array. Starting time (UTC) is given in the upper-left corner. Amplitude scale in cm/sec is shown at lower left with maximum amplitude displayed at the right of each trace.



4-NOV-87 10-43-43

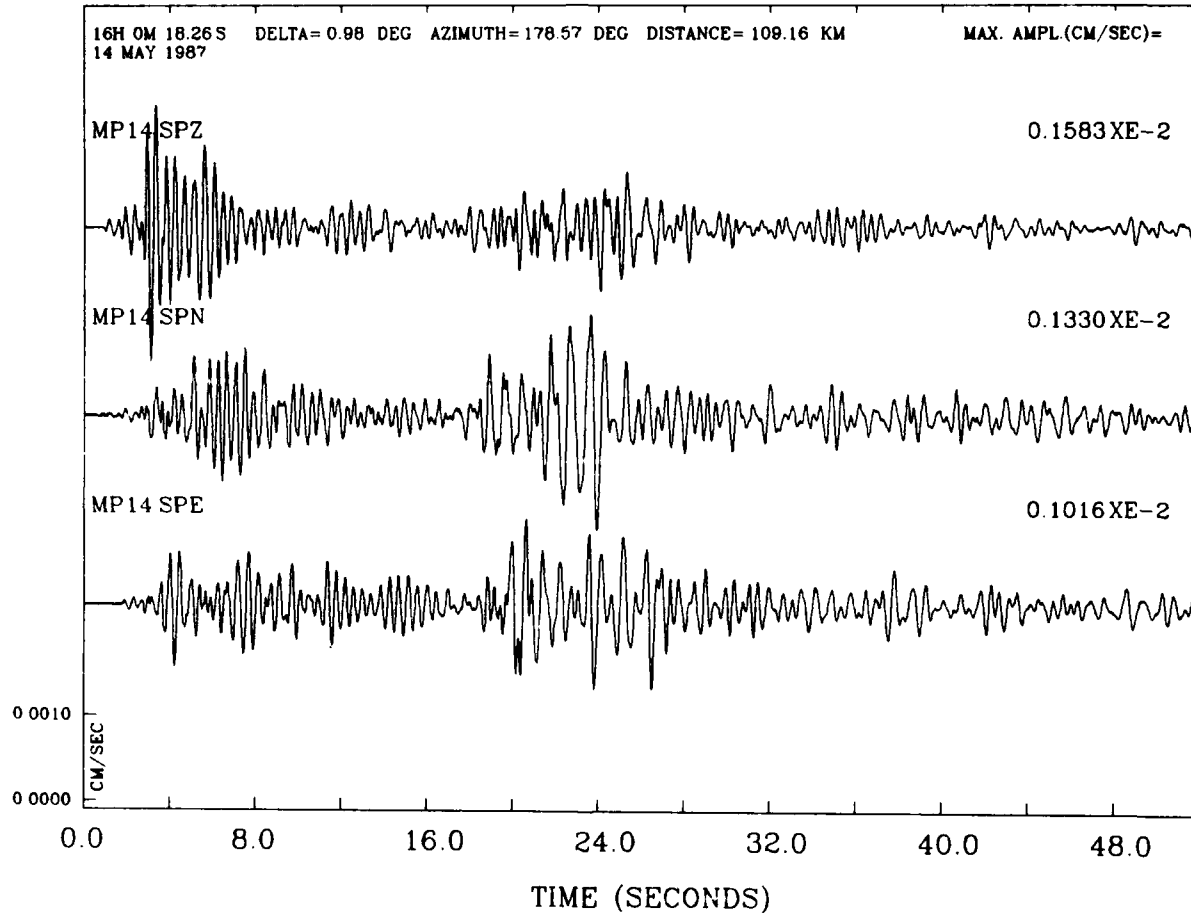
Figure 5. Seismograms recorded at station MP12 of the MISTY PICTURE array. Starting time (UTC) is given in the upper-left corner. Amplitude scale in cm/sec is shown at lower left with maximum amplitude displayed at the right of each trace.



4-NOV-87 10-45-13

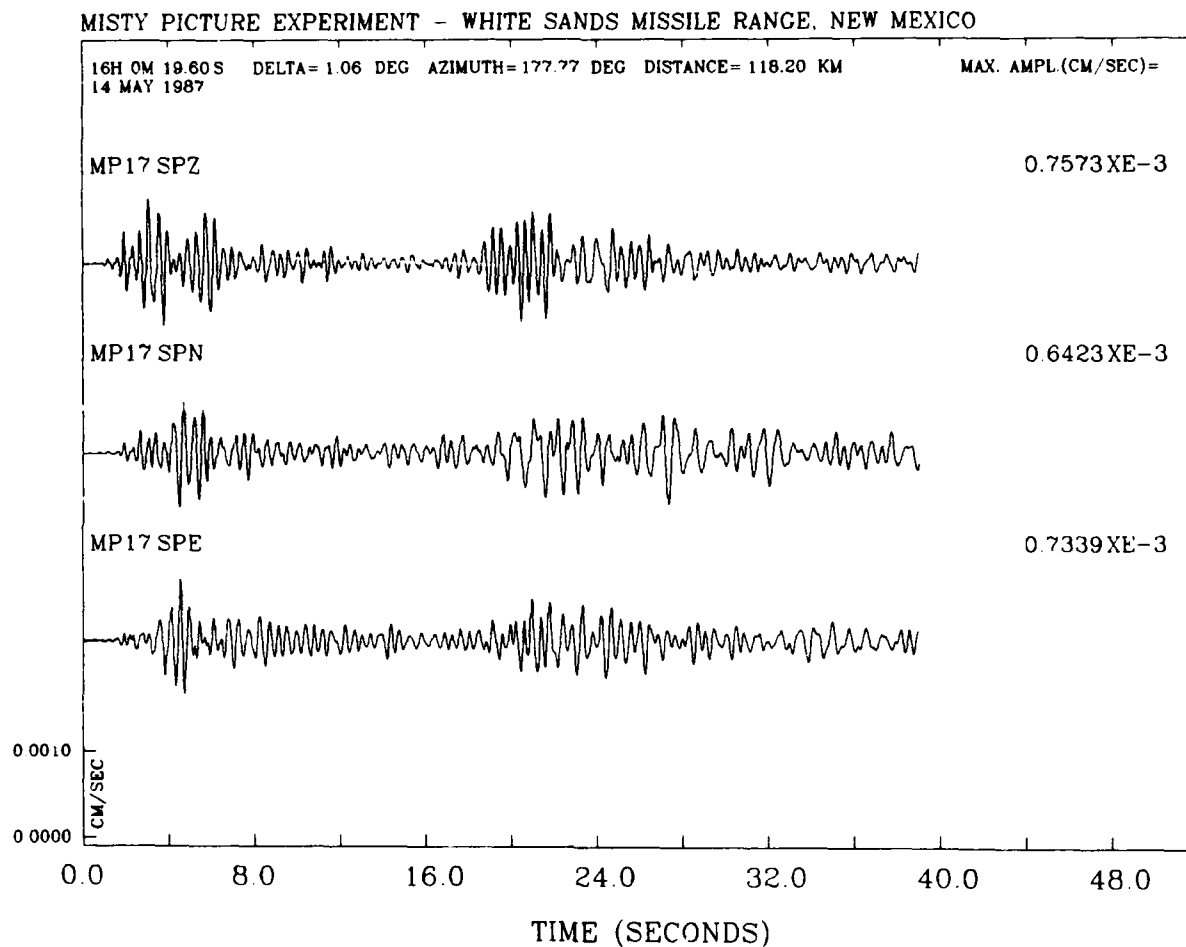
Figure 6. Seismograms recorded at station MP13 OF THE MISTY PICTURE array. Starting time (UTC) is given in the upper-left corner. Amplitude scale in cm/sec is shown at lower left with maximum amplitude displayed at the right of each trace.

MISTY PICTURE EXPERIMENT - WHITE SANDS MISSILE RANGE, NEW MEXICO



4-NOV-87 10-46-44

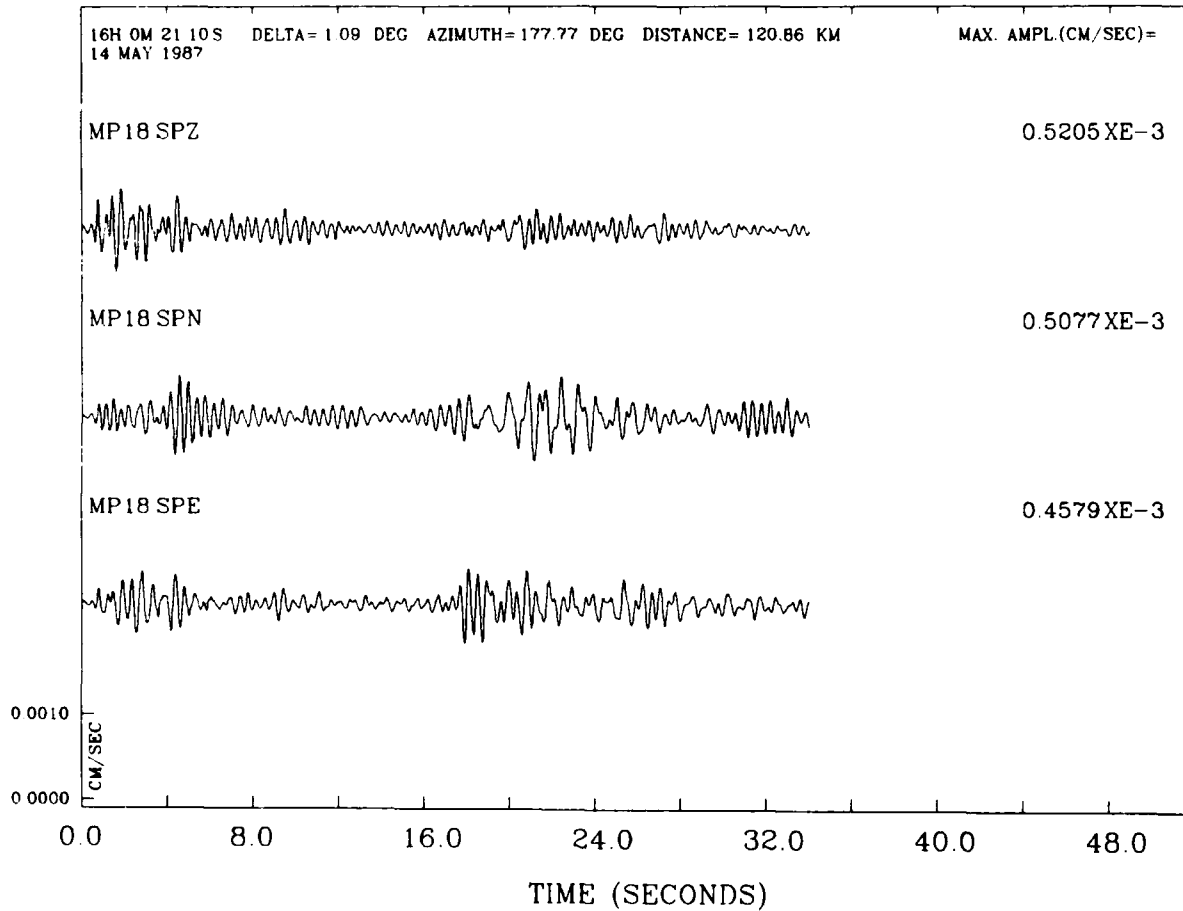
Figure 7. Seismograms recorded at station MP14 of the MISTY PICTURE array. Starting time (UTC) is given in the upper-left corner. Amplitude scale in cm/sec is shown at lower left with maximum amplitude displayed at the right of each trace.



4-NOV-87 10-47-32

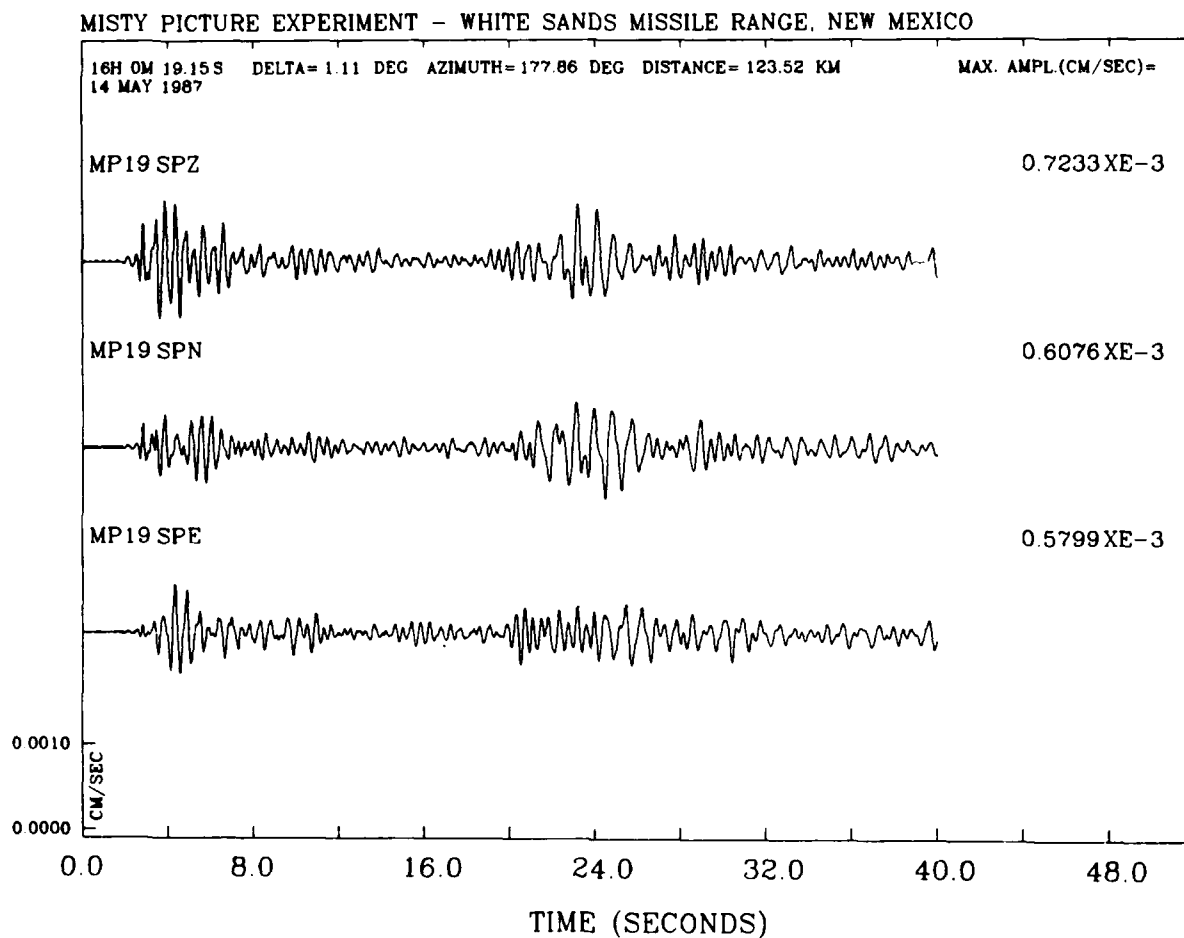
Figure 8. Seismograms recorded at station MP17 of the MISTY PICTURE array. Starting time (UTC) is given in the upper-left corner. Amplitude scale in cm/sec is shown at lower left with maximum amplitude displayed at the right of each trace.

MISTY PICTURE EXPERIMENT - WHITE SANDS MISSILE RANGE, NEW MEXICO



4-NOV-87 10-49-16

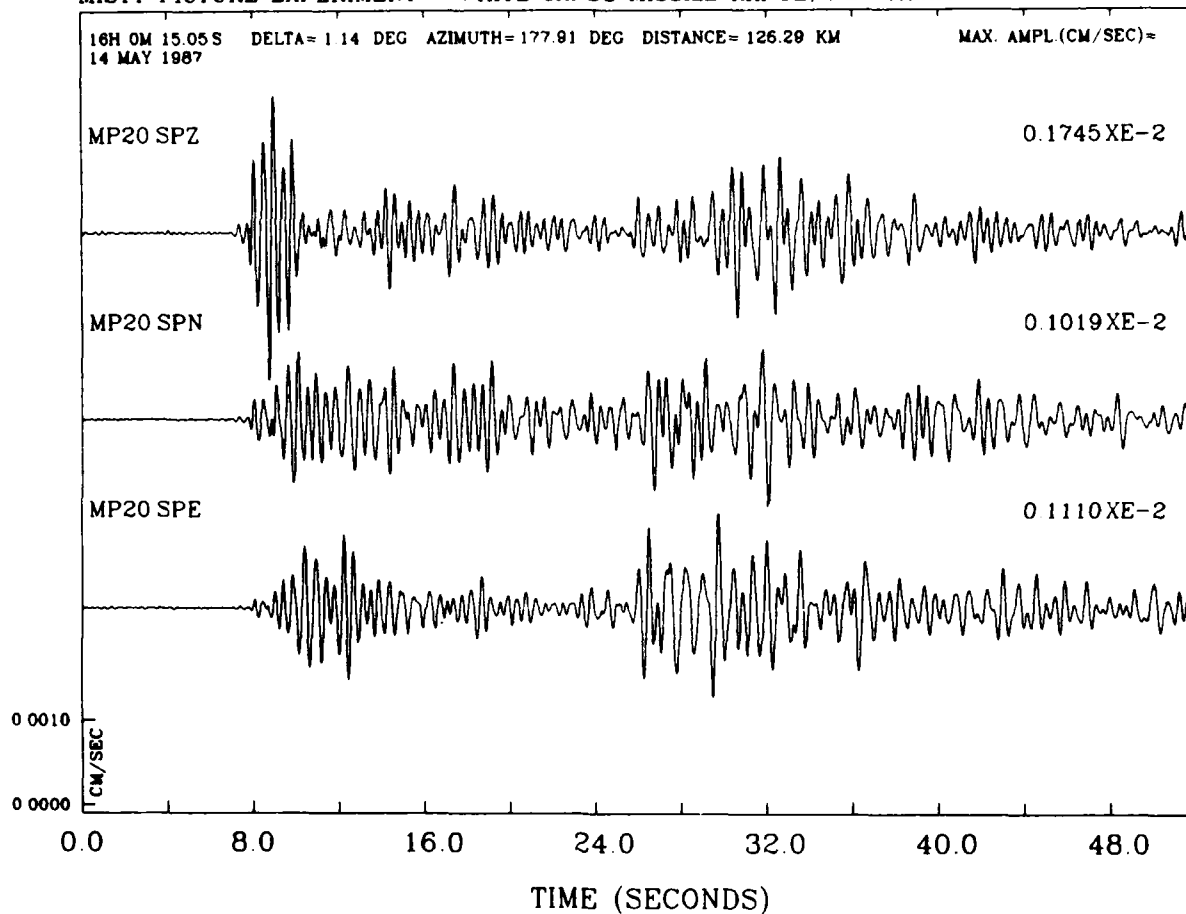
Figure 9. Seismograms recorded at station MP18 of the MISTY PICTURE array. Starting time (UTC) is given in the upper-left corner. Amplitude scale in cm/sec is shown at lower left with maximum amplitude displayed at the right of each trace.



4-NOV-87 10-50-14

Figure 10. Seismograms recorded at station MP19 of the MISTY PICTURE array. Starting time (UTC) is given in the upper-left corner. Amplitude scale in cm/sec is shown at lower left with maximum amplitude displayed at the right of each trace.

MISTY PICTURE EXPERIMENT - WHITE SANDS MISSILE RANGE, NEW MEXICO



4-NOV-87 10-50-59

Figure 11. Seismograms recorded at station MP20 of the MISTY PICTURE array. Starting time (UTC) is given in the upper-left corner. Amplitude scale in cm/sec is shown at lower left with maximum amplitude displayed at the right of each trace.

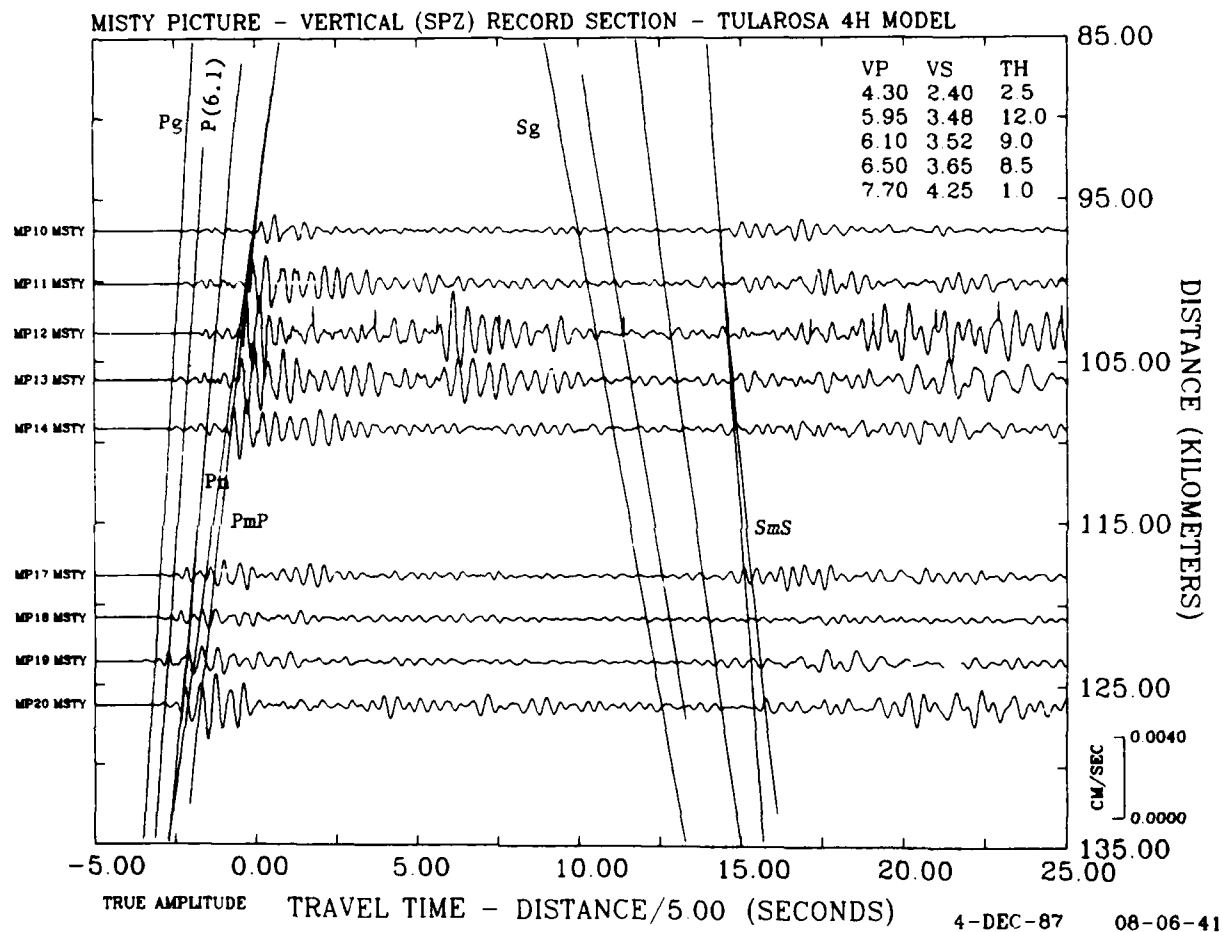


Figure 12. Vertical record section at a 5.0-km/sec reduction velocity. Travel time curves are shown for the crustal model shown in upper right. Phases are discussed in text.

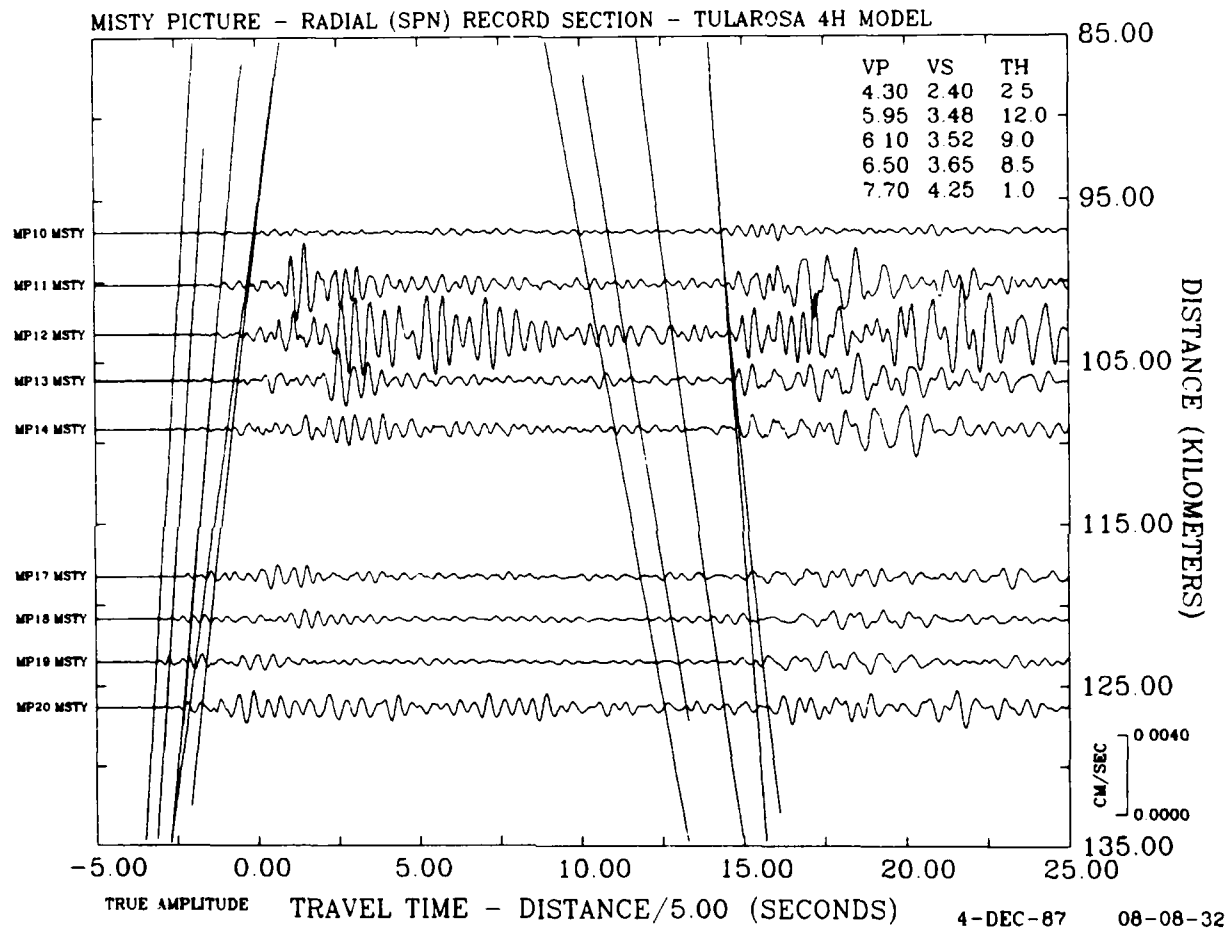


Figure 13. Radial record section. See figure 12 for explanation of phases.

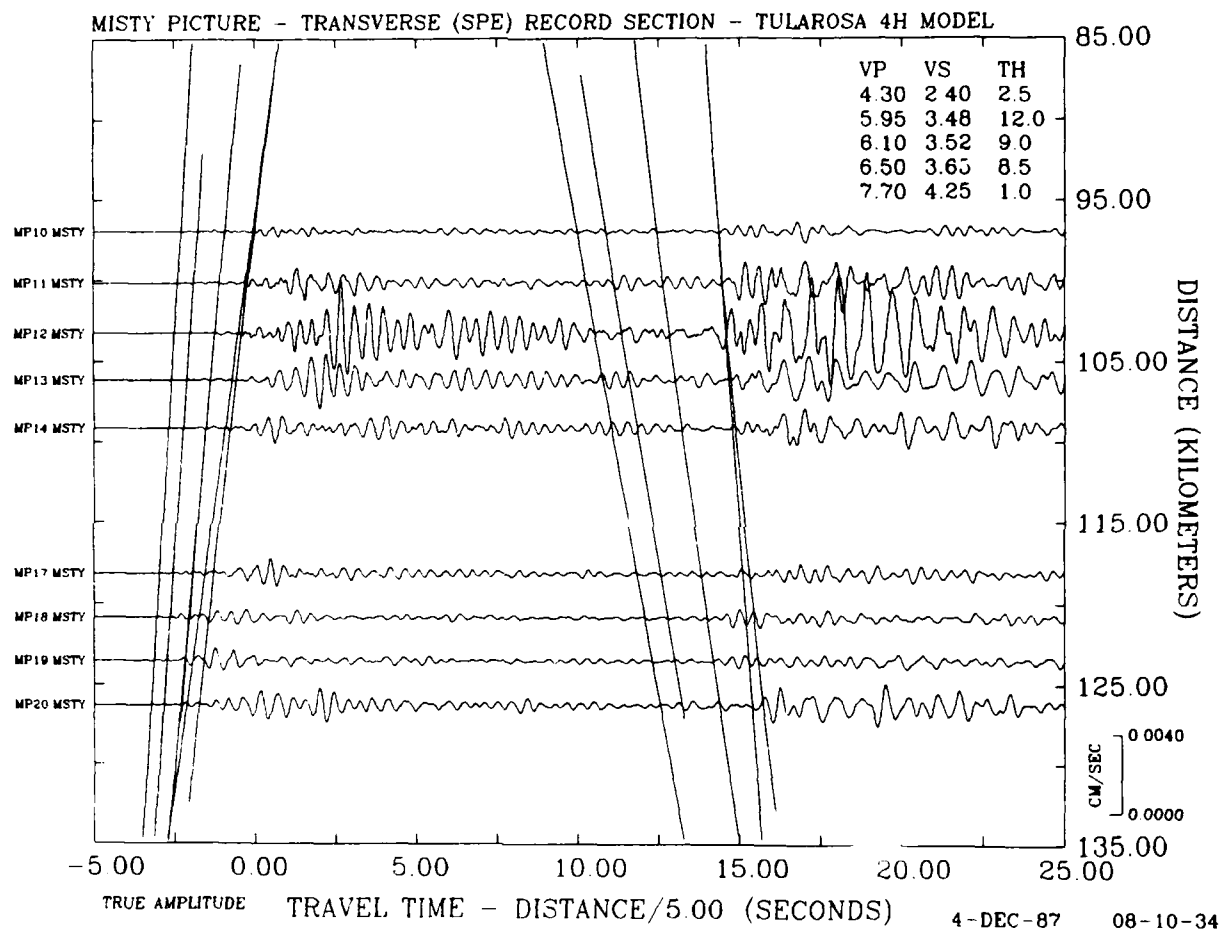


Figure 14. Transverse record section. See figure 12 for explanation of phases.

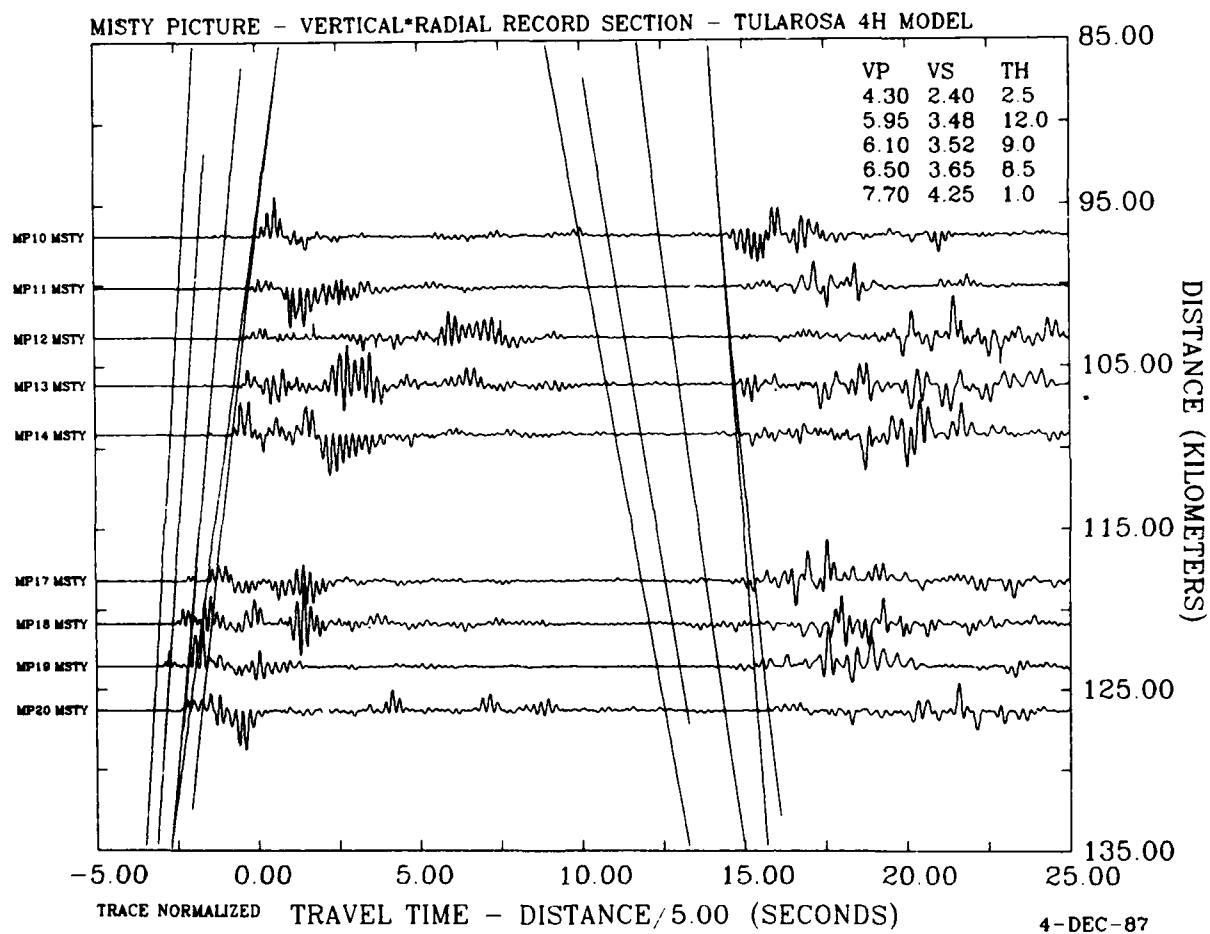


Figure 15. Record section of product of vertical and radial seismograms.